

**Weierstraß-Institut**  
**für Angewandte Analysis und Stochastik**  
**Leibniz-Institut im Forschungsverbund Berlin e. V.**

Preprint

ISSN 0946 – 8633

**Collision detection between robots moving along specified  
trajectories**

Nelson Feyeux<sup>1</sup>, Chantal Landry<sup>2</sup>

submitted: December 10, 2013

<sup>1</sup> Ecole Centrale de Lyon  
36 Avenue Guy de Collongue  
69134 Ecully Cedex  
France  
E-Mail: Nelson.Feyeux@ecl2013.ec-lyon.fr

<sup>2</sup> Weierstrass Institute  
Mohrenstr. 39  
10117 Berlin  
Germany  
E-Mail: chantal.landry@wias-berlin.de

No. 1892  
Berlin 2013



---

2010 *Mathematics Subject Classification.* 51M20, 51K99, 52B10, 68T40.

*Key words and phrases.* Collision detection, distance computation, motion planning, robotics.

This work was partially supported by the German Research Foundation MATHEON.

Edited by  
Weierstraß-Institut für Angewandte Analysis und Stochastik (WIAS)  
Leibniz-Institut im Forschungsverbund Berlin e. V.  
Mohrenstraße 39  
10117 Berlin  
Germany

Fax: +49 30 20372-303  
E-Mail: [preprint@wias-berlin.de](mailto:preprint@wias-berlin.de)  
World Wide Web: <http://www.wias-berlin.de/>

## Abstract

An algorithm to detect collisions between robots moving along given trajectories is presented. The method is a combination of the adaptive dynamic collision checking developed by Schwarzer et al. and Lin and Canny's algorithm, which computes efficiently the distance between two polyhedra. The resulting algorithm is part of a global model that computes the optimal task assignment, sequencing and kinodynamic motion planning in a robotic work-cell.

## 1 Introduction

The application of our research lies in automotive industry and their production lines. A production line is divided into work-cells, which consists of a workpiece, several robots and some obstacles. Typical obstacles are the conveyor belt, which connects the cells to each other. In a work-cell, the robots perform tasks on the same workpiece. The total time taken by the robots to complete all the tasks is called the *makespan* of the work-cell.

To ensure the competitiveness of car manufacturers, the makespan of the work-cells must be as small as possible. The makespan is minimal when the following three points are optimized:

- 1 kinodynamic motion planning of each robot,
- 2 task assignment between the robots,
- 3 sequencing of the tasks of each robot.

The kinodynamic motion planning computes the fastest trajectory that relies two locations and does not collide with the obstacles. Task assignment involves deciding which robot performs which tasks. The sequencing determines in which order the robot executes its assigned tasks. One sequence is defined per robot. The first and last elements of a sequence are the initial position of the robot. The elements in between are task locations. The traversal time of a sequence is the sum of the travel time of the fastest collision-free trajectory between two consecutive elements of the sequence. The travel times are obtained by solving the kinodynamic motion planning problem. The makespan is then equal to the largest traversal time.

The problem of minimizing the makespan is called the *Work-Cell Problem* (WCP). A complete description of (WCP) can be found in [13]. This problem is a typical instance of Vehicle Routing Problem [25]. Therefore, (WCP) is modelled by a directed graph. The nodes of the graph are the task locations and the initial position of the robots. Two nodes are connected by an arc if a robot can move from one node to the other. The weight on the arc is the travel time.

An iterative method is used to solve (WCP). First, a discrete optimization method computes a sequence of tasks for each robot. These sequences are such that the makespan is minimized. By definition of (WCP), the trajectories between two consecutive nodes avoid the obstacles. The collision avoidance between the robots has not been taken into consideration yet. That is why the second step involves detecting such collisions. If the robots hit each other, the algorithm goes back to the first step and looks for new sequences. If no collision occurs, then (WCP) is solved. The aim of this paper is to present how to achieve the second step efficiently.

There exist two classes of collision detection methods: the *static* and the *dynamic* collision detection. The static approach checks if there is a collision between two objects at each time step [19]. The *dynamic* collision checking determines if for all configurations given on a continuous path a collision occurs between the objects. Cameron in [2] compared the static approach with two types of dynamic checking:

- *The space-time approach*: build for each object a volume that represents the spatial occupancy of the object along its trajectory. The volume is obtained by extruding the original configuration of the object.
- *The sweeping approach* [1]: compute the volume swept out by the object.

Once these volumes are built, both methods check a possible intersection between the volume of each object.

Cameron pointed out the advantages and drawbacks of each approach. The static detection is simple, but can miss a collision if the time discretization is too rough. On the other side taking small time steps is time consuming. The choice of a good number of time steps is still a difficult task. The space-time approach is an elegant method. However, extruding the volume can be complicated when the object undergoes rotations and has complex geometry. The sweeping approach has the same drawback. Moreover the technique can detect a collision even though no intersection exists between the objects. In conclusion, none of these methods is the best.

After Cameron's article new techniques have been introduced such as (See Jiménez et al. [12] and Lin and Gottschalk [18] for a good survey)

- *The trajectory parameterization* method [4, 8, 23]: the collision checking is modelled by finding numerically roots of an algebraic polynomial in a single variable  $t$ .
- *The feature-tracking* method [5, 17, 21]: there exist three kinds of features: vertices, edges and faces. The feature-tracking methods involves computing the pair of closest features (one feature per object) and looking if this pair remains separated along the trajectory.
- *The bounding volume hierarchy* (BVH) method [6]: this technique computes first a hierarchy of bounding volumes (spheres [11, 22], oriented bounding boxes [10], axis-aligned bounding boxes [5], rectangular swept sphere [14], ...) to describe each object at various levels of details. Then the algorithm checks for collision by considering first the volumes of the roughest level. If a collision is detected, then the next level is considered and the associated volumes are tested for overlaps. If a pair of volumes in the finest level of detail is overlapping, a collision between the objects occurs. This method is then applied at

given configurations on the trajectory. If all these configurations are collision-free, then no collision occurs between the objects.

As Schwarzer et al. observed in [24], all these methods have drawbacks. The trajectory parameterization technique is computationally expensive and could suffer of numerical problems when the polynomials have high degree. Feature-tracking requires small increments to avoid missing collisions, which can become computationally expensive when working with real robots. (BVH) methods is a static collision detection method. So, (BVH) could miss a collision if the number of time steps is too small.

Schwarzer et al. suggested in [24] a new dynamic collision detection method. They established a sufficient condition to determine if two polyhedra do not collide over a time interval. The condition involves checking if an inequality holds. If the inequality is not satisfied, then the time interval is split into two subintervals and the condition is checked on both subintervals. This method is simple, never fails and adapts automatically the sampling resolution. For all these reasons, we choose to follow Schwarzer et al.'s method.

In Section 2, the input data for the second step in the iterative method to solve (WCP) are presented. In Section 3, Schwarzer et al.'s inequality to determine if a collision occurs between two moving robots is established. The computation of the left hand side of the inequality is given in Section 4, whereas Section 5 is concerned with the right hand side. Finally, numerical results are given in Section 6.

## 2 Input data

Let us consider two robots that we denote, without loss of generality,  $R_1$  and  $R_2$ . Both robots are a two-dimensional convex polyhedron. The robot  $R_1$  is assumed to move from the position  $V_I^1$  to  $V_F^1$ , whereas the robot  $R_2$  goes from  $V_I^2$  to  $V_F^2$  during the same period. We would like to know if  $R_1$  and  $R_2$  collide during this period. In the sequel let  $R_i$  denote the robots  $R_1$  and  $R_2$  in a general way.

The motion of the robots between their initial and final position, is given. As part of (WCP), the trajectory was obtained by solving a kinodynamic motion planning problem [13]. This problem was solved with a time discretization [7]. Therefore, the motion is a discretized trajectory given in the following manner: if  $0 \leq t_1 < \dots < t_n$  denote the time discretization with  $n$  time steps, then the configuration of the robot  $R_i$  at time step  $t_k$  is approximated by the tuple

$$p_i^{(k)} := (G_i^{(k)}, v_i^{(k)}, \theta_i^{(k)}, \mu_i^{(k)}),$$

where  $G_i^{(k)} = (x_i^{(k)}, y_i^{(k)})$  is the position of the center of gravity of the robot,  $v_i^{(k)} = (v_{i,x}^{(k)}, v_{i,y}^{(k)})$  is the velocity of the center of gravity,  $\theta_i^{(k)}$  is the angle of rotation and  $\mu_i^{(k)}$  is the velocity of the angle of rotation. The axis of rotation is placed at the center of gravity of the robot. In particular, we have  $G_i^{(1)} = V_I^i$  and  $G_i^{(n)} = V_F^i$ .

In the sequel, the trajectory must be evaluated at intermediate times. For that purpose, the trajectory is approximated by a linear interpolation. If we consider the time interval  $[t_k, t_{k+1}]$ ,

the intermediate configurations are approximated by

$$\bar{p}_i^{(k)}(t) := \frac{t_{k+1} - t}{t_{k+1} - t_k} p_i^{(k)} + \frac{t - t_k}{t_{k+1} - t_k} p_i^{(k+1)}, \quad \forall t \in [t_k, t_{k+1}]. \quad (1)$$

With each robot, we associate a Cartesian coordinate system  $(G_i, e_x^i, e_y^i)$ ,  $i = 1, 2$ , whose origin is the center of gravity  $G_i$ . The pair  $(e_x^i, e_y^i)$  is the  $x$ - and  $y$ - axes respectively. This coordinate system is called *body frame* according to [15]. A Cartesian coordinate system is also associated to the workspace. This system is named *world frame* and denoted by  $(O, e_x, e_y)$ . The configuration  $p_i^{(k)}$  allows us to represent the robot  $R_i$  at time step  $t_k$  in the world frame. The position of the robot is obtained by rotating the robot counterclockwise of angle  $\theta_i^{(k)}$  and translating it along the vector  $\overrightarrow{OG_i^{(k)}}$ , see Figure 1.

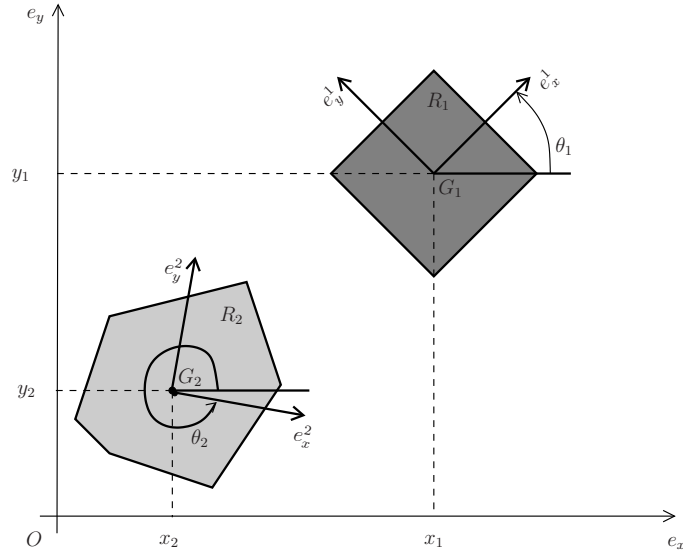


Figure 1: The position of the robot  $R_1$  (resp.  $R_2$ ) in the world frame  $(O, e_x, e_y)$ , is given by its center of gravity  $G_1$  (resp.  $G_2 = (x_2, y_2)$ ) and the rotation angle  $\theta_1$  (resp.  $\theta_2$ ).

Similarly, if  $P_i$  is a vertex of the robot  $R_i$ , whose coordinates are given in the body frame, then the coordinates of  $P_i$  in the world frame at time  $t^{(k)}$  are

$$P_i^{(k)} := \mathcal{R}(\theta_i^{(k)}) P_i + G_i^{(k)}, \quad (2)$$

where

$$\mathcal{R}(\theta_i^{(k)}) = \begin{pmatrix} \cos(\theta_i^{(k)}) & -\sin(\theta_i^{(k)}) \\ \sin(\theta_i^{(k)}) & \cos(\theta_i^{(k)}) \end{pmatrix} \quad (3)$$

is the rotation matrix.

In summary, the approximated trajectory of a robot  $R_i$  is given by a sequence of time steps  $(t_k)_{k=1}^n$  and the associated sequence of configurations  $(p_i^{(k)})_{k=1}^n$ . Since the number and values

of time steps are specific to each robot, we define  $(\tau_k)_{k=1}^n$  and  $(p^{(k)})_{k=1}^n$  as the sequences associated with  $R_1$ , and  $(T_k)_{k=1}^N$  and  $(q^{(k)})_{k=1}^N$  as those with  $R_2$ . Knowing these four sequences, we would like to detect if a collision occurs between  $R_1$  and  $R_2$ .

Since the robots have usually a different time discretization, we need first to classify the time steps  $(\tau_k)_{k=1}^n$  and  $(T_k)_{k=1}^N$  in an ascending order as illustrated in Figure 2. The time interval is then decomposed on subintervals  $[t_l, t_u]$  of type:  $[\tau_\ell, \tau_{\ell+1}]$ ,  $[\tau_\ell, T_j]$ ,  $[T_j, \tau_\ell]$  and  $[T_j, T_{j+1}]$ .

In the next section, we check on each subinterval if a collision between the robots occurs. For that purpose, the configuration of the robots must be evaluated at the boundary of the subinterval  $[t_l, t_u]$ . If  $t_l$  (resp.  $t_u$ ) belongs to  $[\tau_1, \tau_n]$ , then the configuration  $p_l$  (resp.  $p_u$ ) of the robot  $R_1$  is given by the linear interpolation defined in (1). The case  $t_l < \tau_1$  means that the robot  $R_2$  moves during the time interval  $[t_l, \tau_1]$ , whereas the robot  $R_1$  stays at its initial place. In that case, we have  $p_l = p^{(1)}$ . Similarly, the scenario  $t_u > \tau_n$  signifies that the robot  $R_1$  has reached its final destination  $V_F^1$  and the robot  $R_2$  is still moving. Consequently,  $p_u = p^{(n)}$ . In summary, the configuration of robot  $R_1$  at  $t_l$  and  $t_u$  is given by

$$p_s := \begin{cases} p^{(\ell)} & \text{if } t_s = \tau_\ell, \\ p^{(1)} & \text{if } t_s = T_j \text{ and } T_j < \tau_1, \\ \bar{p}^{(\ell)}(T_j) & \text{if } t_s = T_j \text{ and } T_j \in [\tau_\ell, \tau_{\ell+1}], \ell = 1, \dots, n-1, \\ p^{(n)} & \text{otherwise,} \end{cases} \quad (4)$$

where  $s \in \{l, u\}$  and  $\bar{p}^{(\ell)}$  is the linear interpolation defined in (1). For robot  $R_2$ , the configuration at the boundary of the time interval is determined similarly:

$$q_s := \begin{cases} q^{(j)} & \text{if } t_s = T_j, \\ q^{(1)} & \text{if } t_s = \tau_\ell \text{ and } \tau_\ell < T_1, \\ \bar{q}^{(j)}(\tau_\ell) & \text{if } t_s = \tau_\ell \text{ and } \tau_\ell \in [T_j, T_{j+1}], j = 1, \dots, N-1, \\ q^{(N)} & \text{otherwise,} \end{cases} \quad (5)$$

with  $s \in \{l, u\}$ .

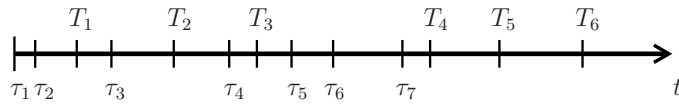


Figure 2: Ascending order of the time steps  $(\tau_k)_{k=1}^n$  and  $(T_k)_{k=1}^N$ . The case  $T_1 > \tau_2$  means that the robot  $R_2$  stays at its initial position  $V_I^2$  when  $R_1$  is moving. Likewise,  $\tau_7 < T_4$  signifies that the robot  $R_1$  has reached its final destination  $V_F^1$ , whereas the robot  $R_2$  is still moving.

### 3 Collision detection algorithm

In this section, the dynamic collision detection method developed by Schwarzer, Saha and Latombe [24] is presented. Let us consider the time subinterval  $[t_l, t_u]$  as defined in Section 2.

Let us remind that the robots are a convex compact polyhedron. Therefore, the word robot is equivalent to polyhedron in the sequel.

The idea of Schwarzer et al. is to compare lower bounds of the distance travelled by the points of the robots during  $[t_l, t_u]$  with an upper bound of the distance between both robots. Let us define the following quantity

- $\eta(t)$  is a non-trivial lower bound of the Hausdorff distance between the robots at time  $t$ . The robots overlap when  $\eta(t) = 0$ . Actually, we consider that the robots overlap when  $\eta(t) < \delta$ , where  $\delta$  is a small positive parameter. In this way, a safety margin around the robots is guaranteed.
- $\lambda_i(t_a, t_b)$  is an upper bound of the length of the curves traced by all points in the robot  $R_i$  between  $t_a$  and  $t_b$ , with  $t_a, t_b \in [t_l, t_u]$ ,  $i \in \{1, 2\}$ .

Schwarzer, Saha and Latombe established the following sufficient condition

**Lemma 1** *Two polyhedra  $R_1$  and  $R_2$  do not collide at any time  $t \in [t_l, t_u]$  if*

$$\lambda_1(t_l, t_u) + \lambda_2(t_l, t_u) < \eta(t_l) + \eta(t_u). \quad (6)$$

Hence, this inequality, which only depends on the boundary values  $t_l$  and  $t_u$ , allows us to know if  $R_1$  and  $R_2$  are collision-free over the whole interval  $[t_l, t_u]$ .

*Proof of Lemma 1* (Schwarzer et al. [24]): Let us assume that the polyhedra  $R_1$  and  $R_2$  overlap at time  $\tilde{t} \in [t_l, t_u]$ . Then, a point  $S_1$  of  $R_1$  must coincide with a point  $S_2$  of  $R_2$  at  $\tilde{t}$ . Let  $\ell_1(t_a, t_b)$  (resp.  $\ell_2(t_a, t_b)$ ) define the length of the curve traced by  $S_1$  (resp.  $S_2$ ) during  $[t_a, t_b]$ . An illustration is given in Figure 3, where  $R_1$  is the white square and  $R_2$  is the black square. The robots are represented at  $t_l$ ,  $\tilde{t}$  and  $t_u$ . Intermediate locations are illustrated with dotted lines. The grey lines are the curves followed by  $S_1$  and  $S_2$ . Because  $S_1$  and  $S_2$  coincide at  $\tilde{t}$ , we have

$$\ell_1(t_l, \tilde{t}) + \ell_2(t_l, \tilde{t}) \geq \eta(t_l), \quad (7)$$

$$\ell_1(\tilde{t}, t_u) + \ell_2(\tilde{t}, t_u) \geq \eta(t_u). \quad (8)$$

Summing (7) and (8), we obtain:

$$\ell_1(t_l, t_u) + \ell_2(t_l, t_u) \geq \eta(t_l) + \eta(t_u). \quad (9)$$

The quantities  $\lambda_1(t_l, t_u)$  and  $\lambda_2(t_l, t_u)$  being an upper bound, we deduce from (9):

$$\lambda_1(t_l, t_u) + \lambda_2(t_l, t_u) \geq \ell_1(t_l, t_u) + \ell_2(t_l, t_u) \geq \eta(t_l) + \eta(t_u),$$

what contradicts the inequality (6). ■

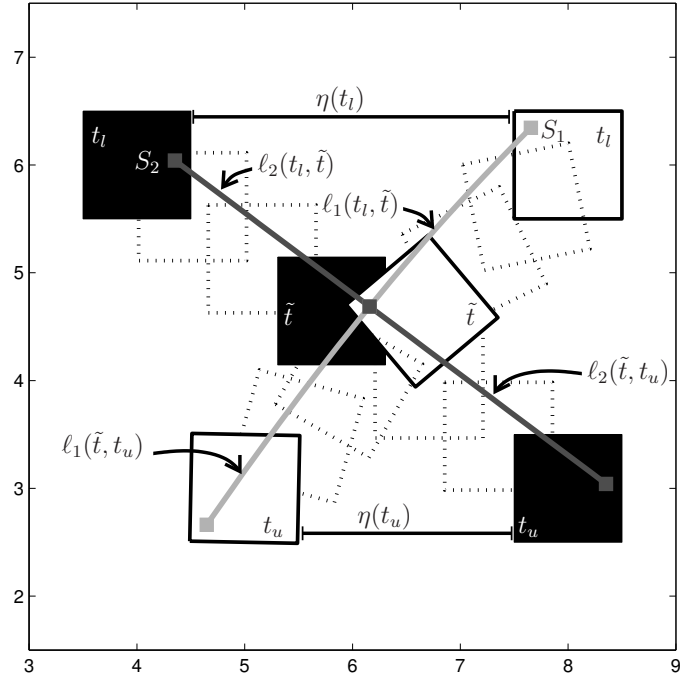


Figure 3: Illustration of the colliding case. The robot  $R_1$  is the white square and the robot  $R_2$  is the black square. The robots collide at time  $\tilde{t}$ .

Table 1: Collision detection algorithm on  $[t_l, t_u]$

```

If  $\eta(t_l) < \delta$  or  $\eta(t_u) < \delta$  then
  return false
else
  return Inequality( $t_l, t_u$ )
end if

where the recursive function Inequality( $t_a, t_b$ ) is

If  $\lambda_1(t_a, t_b) + \lambda_2(t_a, t_b) < \eta(t_a) + \eta(t_b)$  then
  return true
else if  $\eta(\frac{1}{2}(t_a + t_b)) < \delta$  then
  return false
else
  return Inequality( $t_a, \frac{1}{2}(t_a + t_b)$ ) or Inequality( $\frac{1}{2}(t_a + t_b), t_b$ )
end if

```

Lemma 1 is a sufficient condition. Therefore, the reverse of the lemma is not true. We cannot conclude the collision-freeness on  $[t_l, t_u]$ , when the inequality is not satisfied. In that case, the time interval is split into two subintervals  $[t_l, t_m]$  and  $[t_m, t_u]$ , where  $t_m = \frac{1}{2}(t_l + t_u)$ . Then, the lower bound  $\eta(t_m)$  is computed. If  $\eta(t_m) < \delta$ , a collision between the robots is detected. Otherwise, the sufficient condition of Lemma 1 is checked on both subintervals  $[t_l, t_m]$  and  $[t_m, t_u]$ . If the inequality (6) is not satisfied for a subinterval, then the subinterval is divided into two parts again and (6) is tested on each part. This process is repeated until either a collision is detected or all subintervals satisfy (6). The collision detection algorithm between  $R_1$  and  $R_2$  on  $[t_l, t_u]$  is summarized in Table 1, where the output “true” means that  $R_1$  and  $R_2$  are separated and “false” indicates that a collision occurs.

A key point of this collision detection checking is that the algorithm automatically decides whether a time interval must be divided further. Furthermore, the method can never fail. To prove this fact, let us observe first that the upper bounds  $\lambda_i(t_a, t_b) \rightarrow 0$  when  $|t_b - t_a| \rightarrow 0$ . Then, let us distinguish the cases:

- If no collision occurs in  $[t_l, t_u]$ , there exists a constant  $\eta_{\min} \geq \delta > 0$  such that

$$\eta(t) \geq \eta_{\min}, \forall t \in [t_l, t_u].$$

With the bisection, the length of the new subintervals is always smaller. The left-hand side of the inequality (6) becomes smaller with the bisection, whereas the right-hand side remains lower-bounded by  $\eta_{\min}$ . Therefore, there exists a set of subintervals of  $[t_l, t_u]$  such that

- 1 the union of all subintervals is equal to  $[t_l, t_u]$ ,
- 2 the inequality (6) is satisfied on each subinterval.

- If the polyhedra overlap, then there is a time subinterval  $[t_a, t_b] \subseteq [t_l, t_u]$  such that

$$\eta(t) < \delta, \forall t \in [t_a, t_b],$$

since the motion of the polyhedra is continuous. Then, by splitting the time intervals, the inequality (6) remains unsatisfied until the new middle point of the time interval falls into  $[t_a, t_b]$ . Let us illustrate this argument with the situation depicted in Figure 4. The time interval  $[t_a, t_b]$  is represented by the grey segment. The algorithm checks first if the polyhedra collide at  $t_l$  and  $t_u$ . The second step of the algorithm establishes that the inequality (6) is not satisfied. The first bisection is executed by computing  $t_1 = \frac{1}{2}(t_l + t_u)$ . No collision occurs at  $t_1$  since  $\eta(t_1) \geq \delta$ . Inequality (6) may be satisfied on  $[t_l, t_1]$ , but not on  $[t_1, t_u]$ . Consequently, the middle point of  $[t_1, t_u]$ :  $t_2 = \frac{1}{2}(t_1 + t_u)$  is computed. The quantity  $\eta(t_2)$  is larger than  $\delta$ . The bisection is then executed and we obtain the following subintervals  $[t_1, t_2]$  and  $[t_2, t_u]$ . The inequality (6) is not satisfied on  $[t_1, t_2]$ . Next, let us compute  $t_3 = \frac{1}{2}(t_1 + t_2)$  and check if  $\eta(t_3)$  is larger than  $\delta$ . Let us do so on until  $t_4 = \frac{1}{2}(t_3 + t_2)$ . For that point, we have  $\eta(t_4) < \delta$ . The collision is detected.

The algorithm in Table 1 is applied to all intervals  $[t_l, t_u]$  issued from the ordering of  $(\tau_k)_{k=1}^n$  and  $(T_k)_{k=1}^N$ . There exists different techniques to decide in which order the subintervals are

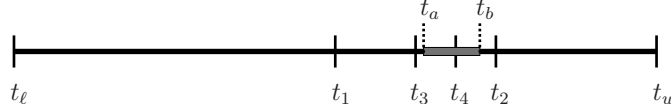


Figure 4: The collision detection algorithm when the polyhedra overlap. The collision is detected by checking if  $\eta(t_4) < \delta$ .

checked, see e.g. [24]. These techniques allow us to detect the collisions faster. In our case, no technique has been implemented since we are interested in detecting the first collision. In the next sections, the computation of the upper and lower bounds in the inequality (6) are presented.

## 4 Computation of the upper bounds $\lambda_1$ and $\lambda_2$

In this section, we are interested in finding an upper bound of the length of the curves traced by the points of the robot between  $t_l$  and  $t_u$ . Schwarzer et al. established in [24] an upper bound when the robot is a planar linkage, whose joints are either revolute or prismatic. In that case, the configuration of the robot is either a rotation angle for the revolute joints or a translation vector for the prismatic joints. In our case, the robot is a polyhedron that moves freely in the workspace. We do not have any joints. The configuration space of the robot  $R_i$  is composed of the position of the center of gravity of the robot,  $G_i$ , the velocity of the center of gravity,  $v_i$ , the rotation angle,  $\theta_i$  and the velocity of the rotation angle  $\mu_i$  as mentioned in Section 2. Hence, we develop our own upper bound, but recommend to use the upper bound of Schwarzer et al. as soon as the robot is a linkage.

Let us consider the subinterval  $[t_l, t_u]$  and two time steps  $t_a, t_b \in [t_l, t_u]$  with  $t_a < t_b$ . The quantity  $\lambda_i(t_a, t_b)$  is defined as an upper bound of the distance travelled by each point of the robot  $R_i$ . Consequently,  $\lambda_i(t_a, t_b)$  satisfies

$$\lambda_i(t_a, t_b) \geq \max_{M_i \in R_i} \int_{t_a}^{t_b} \left\| \frac{d}{dt} \overrightarrow{OM_i}(t) \right\| dt,$$

where  $M_i$  is a point in  $R_i$ .

The right-hand side of the above inequality is hard to calculate exactly, since the robots are rotating. So, let us find an upper bound of the integral by exploiting the definition of  $\overrightarrow{OM_i}$ . This vector can be decomposed as follows (compare (2)):

$$\overrightarrow{OM_i}(t) = \overrightarrow{OG_i}(t) + \overrightarrow{G_iM_i}(t) = \overrightarrow{OG_i}(t) + \mathcal{R}(\theta_i(t)) \overrightarrow{G_iM_i},$$

where  $\mathcal{R}(\theta_i(t))$  is the rotation matrix defined by (3). Note that  $\overrightarrow{G_iM_i}$  is fixed. Then, we have:

$$\begin{aligned} \frac{d}{dt} \overrightarrow{OM_i}(t) &= \frac{d}{dt} \overrightarrow{OG_i}(t) + \frac{d}{dt} \mathcal{R}(\theta_i(t)) \overrightarrow{G_iM_i}, \\ &= v_i(t) + \theta_i'(t) \mathcal{R} \left( \theta_i(t) + \frac{\pi}{2} \right) \overrightarrow{G_iM_i}, \\ &= v_i(t) + \mu_i(t) \mathcal{R} \left( \theta_i(t) + \frac{\pi}{2} \right) \overrightarrow{G_iM_i}. \end{aligned}$$

For all rotation matrices  $\mathcal{R}$  and all vectors  $x$  in  $\mathbb{R}^2$  we have

$$\|\mathcal{R}x\|_2 = \|x\|_2.$$

Using this relation, we obtain:

$$\begin{aligned} \left\| \frac{d}{dt} \overrightarrow{OM_i}(t) \right\|_2 &\leq \|v_i(t)\|_2 + |\mu_i(t)| \left\| \mathcal{R} \left( \theta_i(t) + \frac{\pi}{2} \right) \overrightarrow{G_i M_i} \right\|_2 \\ &= \|v_i(t)\|_2 + |\mu_i(t)| \|\overrightarrow{G_i M_i}\|_2. \end{aligned}$$

Let  $R_{\max,i}$  be the radius of the smallest disc centered at  $G_i$  and containing all vertices of  $R_i$ , that is:

$$R_{\max,i} = \max_{M_i \in R_i} \|\overrightarrow{G_i M_i}\|_2.$$

An illustration is given in Figure 5. Introducing  $R_{\max,i}$  in the last inequality yields:

$$\left\| \frac{d}{dt} \overrightarrow{OM_i}(t) \right\|_2 \leq \|v_i(t)\|_2 + |\mu_i(t)| R_{\max,i}.$$

Let us now integrate the above relation on both sides:

$$\int_{t_a}^{t_b} \left\| \frac{d}{dt} \overrightarrow{OM_i}(t) \right\|_2 dt \leq \int_{t_a}^{t_b} \|v_i(t)\|_2 dt + R_{\max,i} \int_{t_a}^{t_b} |\mu_i(t)| dt. \quad (10)$$

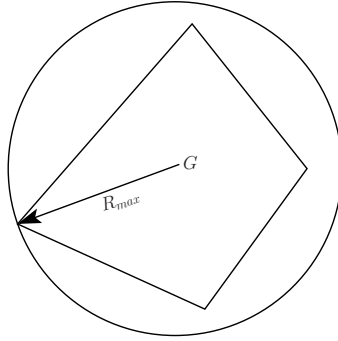


Figure 5: Disc of radius  $R_{\max}$  and center  $G$  that contains the polyhedron.

The values of  $\mu_i$  and  $v_i$ ,  $i = 1, 2$ , are given according to the following linear interpolation

$$\begin{aligned} \mu_i(t) &= a(t) \mu_i(t_a) + (1 - a(t)) \mu_i(t_b), \\ v_i(t) &= a(t) v_i(t_a) + (1 - a(t)) v_i(t_b), \quad \text{with } a(t) = \frac{t_b - t}{t_b - t_a} \in [0, 1]. \end{aligned} \quad (11)$$

The integrals in the right-hand side of (10) become

$$\begin{aligned} \int_{t_a}^{t_b} \|v_i(t)\|_2 &= \int_{t_a}^{t_b} \|a(t)v_i(t_a) + (1 - a(t))v_i(t_b)\|_2 dt, \\ &\leq \|v_i(t_a)\|_2 \int_{t_a}^{t_b} a(t) dt + \|v_i(t_b)\|_2 \int_{t_a}^{t_b} (1 - a(t)) dt, \\ &= \frac{1}{2}(t_b - t_a)(\|v_i(t_a)\|_2 + \|v_i(t_b)\|_2). \end{aligned}$$

Similarly, we have

$$\begin{aligned} \int_{t_a}^{t_b} |\mu_i(t)| &\leq |\mu_i(t_a)| \int_{t_a}^{t_b} a(t) dt + |\mu_i(t_b)| \int_{t_a}^{t_b} (1-a(t)) dt, \\ &= \frac{1}{2}(t_b - t_a)(|\mu_i(t_a)| + |\mu_i(t_b)|). \end{aligned}$$

Finally, we get

$$\int_{t_a}^{t_b} \left\| \frac{d}{dt} \overrightarrow{OM}_i(t) \right\| dt \leq \frac{1}{2}(t_b - t_a)(R_{\max,i}(|\mu_i(t_a)| + |\mu_i(t_b)|) + \|v_i(t_a)\|_2 + \|v_i(t_b)\|_2), \quad i = 1, 2.$$

We define the upper bound  $\lambda_i(t_a, t_b)$  as the right-hand side of the above inequality:

$$\lambda_i(t_a, t_b) := \frac{1}{2}(t_b - t_a) (R_{\max,i}(|\mu_i(t_a)| + |\mu_i(t_b)|) + \|v_i(t_a)\|_2 + \|v_i(t_b)\|_2). \quad (12)$$

In this formula, the terms  $\mu_i(t_a)$ ,  $\mu_i(t_b)$ ,  $v_i(t_a)$  and  $v_i(t_b)$  come also from a linear interpolation. Since  $[t_a, t_b] \subseteq [t_l, t_u]$ , we have

$$\begin{aligned} \mu_i(t_a) &= b(t_a) \mu_i(t_l) + (1 - b(t_a)) \mu_i(t_u), \\ \mu_i(t_b) &= b(t_b) \mu_i(t_l) + (1 - b(t_b)) \mu_i(t_u), \\ v_i(t_a) &= b(t_a) v_i(t_l) + (1 - b(t_a)) v_i(t_u), \\ v_i(t_b) &= b(t_b) v_i(t_l) + (1 - b(t_b)) v_i(t_u), \quad \text{with } b(t) = \frac{t_u - t}{t_u - t_l} \in [0, 1], \end{aligned}$$

and

$$\begin{aligned} p_l &= (G_1(t_l), v_1(t_l), \theta_1(t_l), \mu_1(t_l)), & p_u &= (G_1(t_u), v_1(t_u), \theta_1(t_u), \mu_1(t_u)), \\ q_l &= (G_2(t_l), v_2(t_l), \theta_2(t_l), \mu_2(t_l)), & q_u &= (G_2(t_u), v_2(t_u), \theta_2(t_u), \mu_2(t_u)) \end{aligned}$$

derive from (4)-(5).

**Remark 1** *The upper bound  $\lambda_i(t_a, t_b)$  tends to zero when  $|t_b - t_a|$  tends to zero. This fact was used to justify the convergence of the collision detection algorithm at the end of Section 3.*

## 5 Computation of the lower bound $\eta$

The function  $\eta$  in the inequality (6) is defined as a non-trivial lower bound of the real distance between two polyhedra. As in [5, 21], a two-phase approach is considered. This approach is composed of a *broad phase* and a *narrow phase*. In the broad phase, the polyhedra are approximated by a simple bounding volume such as an axis-aligned box or a sphere. The lower bound  $\eta$  is defined as the distance between the bounding volumes. As long as the bounding volumes

are disjoint, the broad phase is applied. Once the bounding volumes overlap, the narrow phase is used. This phase computes the exact distance between the polyhedra. Thus the two-phase approach induces a minimal cost in the computation of  $\eta$  since the exact distance is determined only when the polyhedra are close to each other. If the robots would have a more complex geometry, then a hierarchy of bounding volumes would be defined such as in [5, 10, 11, 14, 22].

In our two-dimensional case, we define the bounding volume of the broad phase as the smallest disc surrounding the polyhedron and whose center is the center of gravity of the polyhedron. An illustration is given in Figure 5. Then,  $\eta$  is defined as the distance between the two disks, i.e.:

$$\eta(t) = \max(\|G_1 G_2(t)\|_2 - R_{\max,1} - R_{\max,2}, 0), \quad (13)$$

where  $G_i$  and  $R_{\max,i}$  are respectively the center and the radius of the disc  $\mathcal{D}_i$  surrounding the robot  $R_i$ ,  $i = 1, 2$ .

This distance is smaller than the real distance between two polyhedra, but automatically calculated once  $G_i$  and  $R_{\max,i}$  are known. The radius  $R_{\max,i}$ ,  $i = 1, 2$ , are constant, whereas the position of the center  $G_i$ ,  $i = 1, 2$ , evolves in time. The components of  $G_i$  at  $t \in [t_l, t_u]$  is given, as mentioned in the previous sections, by the linear interpolation:

$$G_i(t) = b(t)G_i(t_l) + (1 - b(t))G_i(t_u), \quad \forall t \in [t_l, t_u],$$

with  $b(t) = \frac{t_u - t}{t_u - t_l}$  and  $G_i(t_l), G_i(t_u)$  derive from (4)-(5).

In the narrow phase, the exact distance between the robots is computed. Two main methods exist for distance calculation. The first method is Gilbert, Johnson and Keerthi's algorithm published in 1988 [9] and referred as *GJK*. This algorithm computes the Hausdorff distance of the Minkowski difference  $R_2 - R_1$  from the origin. The second method is Lin and Canny's algorithm [16, 17]. This algorithm tracks the closest pair of features between the polyhedra, where the features of a polyhedron are its vertices, its edges and its faces located on its boundary. Several extensions of both approaches exist such as *Enhanced GJK* [3], *I-collide* [5] and *V-Clip* [20]. We choose to follow Lin and Canny's algorithm since the approach is fast, easy to implement and perfectly suited when polyhedra move slightly between two time steps, as it is the case with the robots  $R_1$  and  $R_2$ .

In two dimensions, the features of a convex polyhedron are the vertices and the edges of the polyhedron. As described in [15], the vertices of the polyhedron are given in counterclockwise order. Let  $m$  be number of vertices of the polyhedron. Let  $E_i$  be the edge going from the vertex  $P_i$  to  $P_{\text{mod}(i,m)+1}$  for  $1 \leq i \leq m$ , where  $\text{mod}(i, m)$  means  $i$  modulo  $m$ . For simplicity, we write the vertex  $P_{\text{mod}(i,m)+1}$  as  $P_{fo(i)}$ , where  $fo$  is the following transformation

$$\begin{aligned} fo : \{1, \dots, m\} &\rightarrow \{1, \dots, m\} \\ b &\mapsto fo(i) = \text{mod}(i, m) + 1. \end{aligned}$$

More generally, the edge  $E_i$ ,  $i = 1, \dots, m$  is an open subset defined as follows

$$E_i = \{x \in \mathbb{R}^2 \mid x = P_i + k e_i, k \in (0, 1)\},$$

where  $e_i = \begin{pmatrix} e_{i,x} \\ e_{i,y} \end{pmatrix} = \overrightarrow{P_i P_{fo(i)}}$ . Hence, the vertices  $P_i$  and  $P_{fo(i)}$  do not belong to the edge.

With this definition, the interior of the convex polyhedron is always located on the left side of the edges as illustrated in Figure 6-(a). Finally, let  $n_i$  be the outward normal vector to edge  $E_i$  whose components stemmed from the vector  $e_i$  as follows

$$n_i = \begin{pmatrix} e_{i,y} \\ -e_{i,x} \end{pmatrix}, \forall i = 1, \dots, m.$$

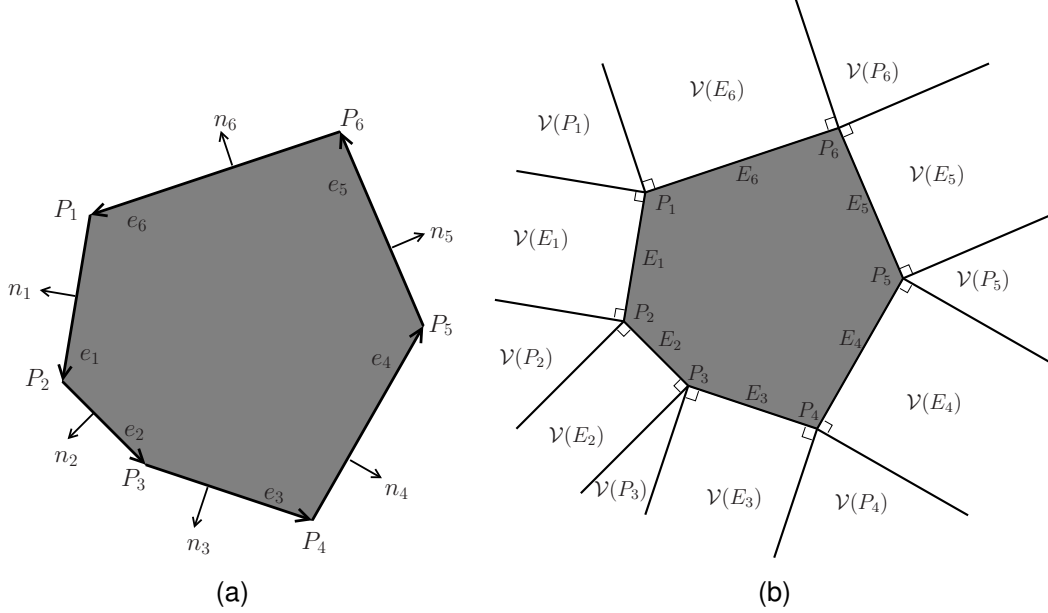


Figure 6: (a) The vertices  $P_i$ ,  $i = 1, \dots, 6$ , of the polyhedron are given in counterclockwise order. The edges  $E_i$ ,  $i = 1, \dots, 6$ , are generated by the direction vector  $e_i$ , which connects the tail  $P_i$  to the head  $P_{fo(i)}$  of the edge. The vectors  $n_i$ ,  $i = 1, \dots, 6$ , are the outward normal vectors to the edges. (b) The Voronoi region of the vertices  $P_i$  and of the edges  $E_i$ ,  $i = 1, \dots, 6$ .

Let  $f_k$  denote a feature of a convex polyhedron  $R$ . With each feature, a Voronoi region is associated. The Voronoi region of  $f_k$  is the set of points that are located outside  $R$  and closer to  $f_k$  than any other features of  $R$ . If  $\mathcal{V}(f_k)$  denotes the Voronoi region of  $f_k$ , then we have:

$$\mathcal{V}(f_k) = \{x \in \mathbb{R}^2 \setminus R \mid d(x, f_k) \leq d(x, f_j), \forall j \neq k\},$$

where the distance function is defined as:  $d(x, f) = \inf\{\|x - a\|_2 \mid a \in f\}$ . In two dimensions, the Voronoi region of a vertex  $P_i$  of  $R$  is the area contained between the half-lines that start from  $P_i$  and are perpendicular to the edges for which  $P_i$  is an endpoint. The Voronoi region of an edge  $E_i$  is the region located above the edge and between the half-lines that start from the endpoints of the edge  $E_i$  and are perpendicular to  $E_i$ . Hence, the Voronoi regions form a partition of  $\mathbb{R}^2 \setminus R$ . An illustration of the Voronoi region of all features in polyhedron  $R$  is given in Figure 6-(b).

The distance between the compact convex polyhedra  $R_1$  and  $R_2$  is

$$d_R(R_1, R_2) = \min_{S_a \in R_1, S_b \in R_2} \|\overrightarrow{S_a S_b}\|_2.$$

Since  $R_1$  and  $R_2$  are compact, the minimum is reached. A pair of points that achieves the minimum is called the *pair of closest points*. This pair may not be unique. Lin and Canny's algorithm tracks the pair of features that contains the closest points. This pair of features is named the *closest pair of features* and found when the following conditions are satisfied:

**Theorem 1** *Let  $R_1$  and  $R_2$  be disjoint compact convex polyhedra. Let  $S_a$  and  $S_b$  be the closest points between the feature  $f_a$  of  $R_1$  and  $f_b$  of  $R_2$ . If  $S_a \in \mathcal{V}(f_b)$  and  $S_b \in \mathcal{V}(f_a)$ , then  $(S_a, S_b)$  is the pair of closest points between  $R_1$  and  $R_2$  and  $(f_a, f_b)$  is the closest pair of features.*

The proof of this theorem can be found in [16]. Lin and Canny's algorithm starts with an initial pair of features and loops on the following three steps until the conditions in Theorem 1 are fulfilled:

- 1 compute the pair of closest points  $(S_a, S_b)$  between the features,
- 2 test if  $S_a \in \mathcal{V}(f_b)$ ,
- 3 test if  $S_b \in \mathcal{V}(f_a)$ .

If both tests succeed, then Theorem 1 implies that the pair  $(S_a, S_b)$  is the closest pair of points and the distance between  $R_1$  and  $R_2$  is equal to  $\|\overrightarrow{S_a S_b}\|_2$ . On the contrary, if  $S_a \notin \mathcal{V}(f_b)$ , then there exists a feature  $f'_b$  of  $R_2$  that is closer to  $S_a$  than  $f_b$ . The pair  $(f_a, f'_b)$  is the new candidate pair and the method continues with the first step of the loop, i.e. the computation of the pair of closest points between  $f_a$  and  $f'_b$ . Similarly, if  $S_b \notin \mathcal{V}(f_a)$ , there exists a feature  $f'_a$  of  $R_1$  that is closer to  $S_b$  than  $f_a$  and a new pair of features is to be tested. Hence, Lin and Canny's algorithm builds a sequence of pair of features whose next candidate is always closer to the previous one. The algorithm stops when Theorem 1 is satisfied or a collision is detected. A sketch of the algorithm is given in Figure 7.

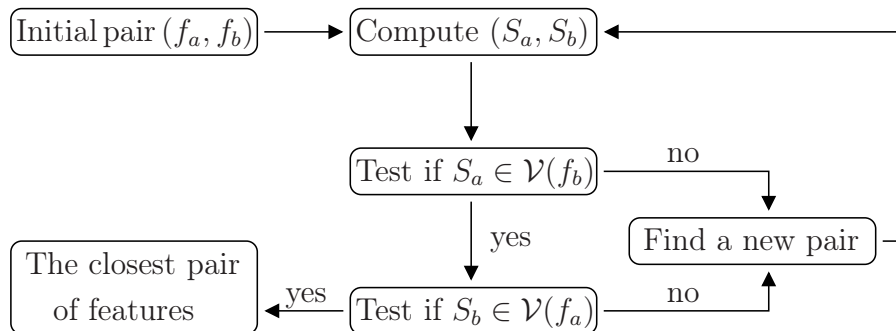


Figure 7: Lin and Canny's algorithm.

In two dimensions, only four kinds of pair of features exist: Vertex-Vertex, Vertex-Edge, Edge-Vertex and Edge-Edge. In the next subsections, we present our two-dimensional version of Lin and Canny's algorithm. We establish how to check if a point belongs to the Voronoi region of a feature and how to choose the next pair of features.

## 5.1 Case Vertex-Vertex

Let us start with the first case, where the pair of features is the vertices  $(P_a, P_b)$ . An illustration is given in Figure 8, where the pair of vertices is  $(P_5, Q_1)$ . In this first case, the pair of closest points between the features is naturally the pair of features itself. The next step in the loop of Lin and Canny's algorithm is to check if  $P_a \in \mathcal{V}(P_b)$ . By definition, the Voronoi region of  $\mathcal{V}(P_b)$  is the area between the half-lines starting at  $P_b$  and perpendicular to the preceding edge,  $E_{\text{mod}(b-2, m)+1}$ , and the following edge,  $E_b$ , of the vertex  $P_b$  (compare Figure 6-(a)). For simplicity, we write the preceding edge as  $E_{pr(b)}$ , where  $pr$  is the following transformation

$$\begin{aligned} pr : \{1, \dots, m\} &\rightarrow \{1, \dots, m\} \\ i &\mapsto pr(i) = \text{mod}(i - 2, m) + 1. \end{aligned}$$

The point  $P_a$  belongs to  $\mathcal{V}(P_b)$  if and only if  $P_a$  is located in the lower half-plane  $\pi(P_b, e_b)$  generating by the outward normal vector  $e_b$  and the point  $P_b$ , and in the lower half-plane  $\pi(P_b, -e_{pr(b)})$ .

Let us consider the orthogonal projection of  $P_a$  onto the line  $\ell(e_b, P_b)$  defined by the direction vector  $e_b$  and the point  $P_b$ . By definition, the orthogonal projection, noted  $S$ , is given by

$$S = P_b + \alpha_b e_b, \quad \text{with } \alpha_b = \frac{\overrightarrow{P_b P_a} \cdot e_b}{\|e_b\|_2^2}. \quad (14)$$

If the projection coefficient  $\alpha_b \leq 0$ , then the projection  $S$  is located before  $P_b$  on the line  $\ell(e_b, P_b)$ . If  $\alpha_b \in (0, 1)$ , then the projection is between  $P_b$  and  $P_{fo(b)}$ , and if  $\alpha_b \geq 1$ , then  $S$  is located after  $P_{fo(b)}$  on the line  $\ell(e_b, P_b)$ . Consequently, the point  $P_a$  belongs to  $\pi(P_b, e_b)$  if and only if its projection coefficient is negative. Similarly, the point  $P_a$  belongs to  $\pi(P_b, e_{pr(b)})$  if and only if the projection of  $P_a$  on the line  $\ell(e_{pr(b)}, P_{pr(b)})$  is located after the point  $P_b$ . In other words,  $P_a \in \pi(P_b, e_{pr(b)})$  if and only if the projection coefficient is larger than 1. Therefore,  $P_a \in \mathcal{V}(P_b)$  when:

$$\alpha_b = \frac{\overrightarrow{P_b P_a} \cdot e_b}{\|e_b\|_2^2} \leq 0 \quad \text{and} \quad \alpha_{pr(b)} = \frac{\overrightarrow{P_{pr(b)} P_a} \cdot e_{pr(b)}}{\|e_{pr(b)}\|_2^2} \geq 1. \quad (15)$$

To avoid numerical problems, the above inequalities are relaxed as follows

$$\alpha_b \leq \delta_c, \quad \text{and} \quad \alpha_{pr(b)} \geq 1 - \delta_c. \quad (16)$$

where  $\delta_c$  is a small positive parameter.

Similarly, we check if the vertex  $P_b$  belongs to the Voronoi region  $\mathcal{V}(P_a)$ . If so, the pair of features  $(P_a, P_b)$  is the closest pair. In Figure 8-(a), we can observe that the vertex  $P_5$  belongs to the lower half-planes  $\pi(Q_1, e_1)$  and  $\pi(Q_1, -e_3)$ . We deduce that  $P_5 \in \mathcal{V}(Q_1)$ . In Figure 8-(b), the vertex  $Q_1$  does not belong to  $\mathcal{V}(P_5)$  since  $Q_1$  is located above the half-plane  $\pi(P_5, -e_4)$ . The second inequality in (16) is therefore violated. In fact,  $Q_1$  is closer to the feature  $e_4$  than to  $P_5$ . The pair of features is updated to  $(E_4, Q_1)$ , the violated condition in (16) indicating the new feature to consider. The algorithm to handle the case Vertex-Vertex is summarized in Table 2 where the projection coefficients  $\alpha_a$ ,  $\alpha_{pr(a)}$ ,  $\alpha_b$  and  $\alpha_{pr(b)}$  are computed according to (14) and (15).

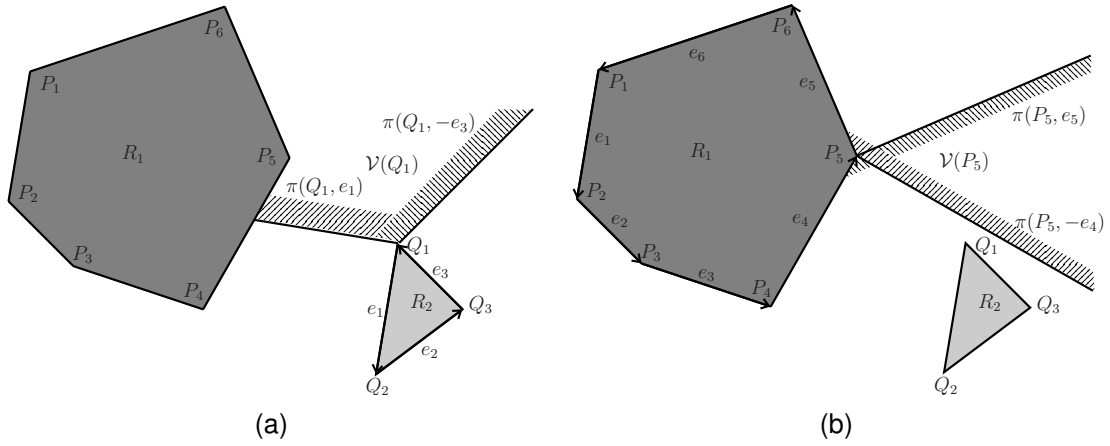


Figure 8: The pair of features  $(P_5, Q_1)$  is considered. (a) The vertex  $P_5$  belongs to  $\mathcal{V}(Q_1)$  since  $P_5$  is located in the lower half-planes  $\pi(Q_1, e_1)$  and  $\pi(Q_1, -e_3)$ . (b) The vertex  $Q_1$  does not belong to  $\mathcal{V}(P_5)$  since  $Q_1$  is located above the lower half-plane  $\pi(P_5, -e_4)$ . The vertex  $Q_1$  is actually closer to the edge  $e_4$  than to the vertex  $P_5$ .

Table 2: Algorithm “Vertex( $P_a$ )-Vertex( $P_b$ )”

```

If  $\alpha_b > \delta_c$  then
  return new pair  $(P_a, E_b)$ 
Else if  $\alpha_{pr(b)} < 1 - \delta_c$  then
  return new pair  $(P_a, E_{pr(b)})$ 
Else
  If  $\alpha_a > \delta_c$  then
    return new pair  $(E_a, P_b)$ 
  Else if  $\alpha_{pr(a)} < 1 - \delta_c$  then
    return new pair  $(E_{pr(a)}, P_b)$ 
  Else
    return  $(P_a, P_b)$  is the closest pair
  End if
End if

```

## 5.2 Case Edge-Vertex

Let us assume that the feature  $E_a$  is an edge of  $R_1$  and the feature  $P_b$  is a vertex of  $R_2$ . To apply Theorem 1, one needs to compute first the closest points  $S_a$  and  $S_b$  between the pair of features  $(E_a, P_b)$ . Then,  $S_a \in \mathcal{V}(P_b)$  and  $S_b \in \mathcal{V}(E_a)$  are checked. The former relation is verified thanks to (16), whereas the point  $S_b$  belongs to  $\mathcal{V}(E_a)$  if

$$S_b \text{ lies in the lower half-plane } \pi(P_a, -e_a), \quad (17)$$

$$S_b \text{ lies in the lower half-plane } \pi(P_{fo(a)}, e_a), \quad (18)$$

$$S_b \text{ is above the edge } E_a. \quad (19)$$

These three conditions follow directly from the definition of the Voronoi region of an edge.

Since  $P_b$  is a vertex, the point  $S_b$  is equal to  $P_b$ . For the point  $S_a$ , one needs to compute the orthogonal projection of  $S_b$  onto the line  $\ell(e_a, P_a)$  defined by the direction vector  $e_a$  and the point  $P_a$ . By definition, the orthogonal projection, noted  $S$ , is given by

$$S = P_a + \alpha e_a, \text{ with } \alpha = \frac{\overrightarrow{P_a S_b} \cdot e_a}{\|e_a\|_2^2}. \quad (20)$$

If  $\alpha \leq 0$ , then the projection  $S$  is located before  $P_a$  on the line  $\ell(e_a, P_a)$ . This means that the vertex  $P_b$  is closer to the vertex  $P_a$  than to the edge  $E_a$ . Hence, the pair of features  $(P_a, P_b)$  is a closer pair than  $(E_a, P_b)$ . This case is illustrated in Figure 9-(a), where  $P_b$  is  $Q_1$  and  $E_a$  is the edge  $E_5$ . With the help of the figure, we can notice that  $\alpha \leq 0$  also means that  $P_b$  lies above the lower half-plane  $\pi(P_a, -e_a)$ . Consequently, the vertex  $P_b$  cannot belong to  $\mathcal{V}(E_a)$ . The case,  $\alpha \leq 0$  implies that  $P_b \notin \mathcal{V}(E_a)$  and the new candidate pair of features is  $(P_a, P_b)$ . The case  $\alpha \geq 1$  is treated similarly. It follows that  $P_b \notin \mathcal{V}(E_a)$  and the new candidate pair is  $(P_{fo(a)}, P_b)$ .

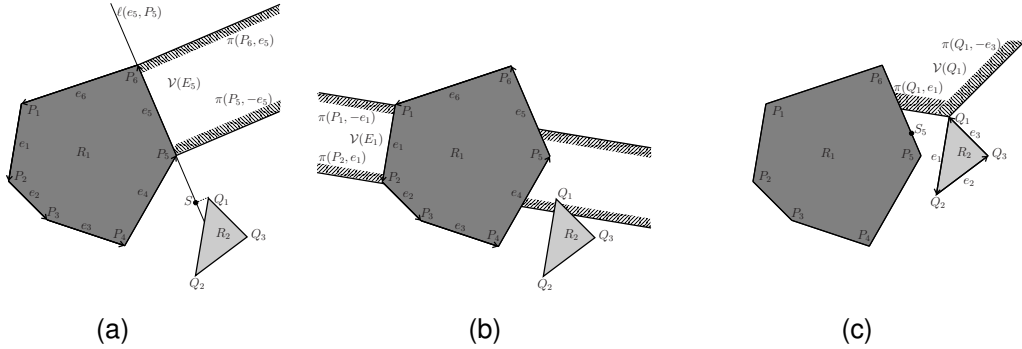


Figure 9: (a) The pair  $(E_5, Q_1)$  is considered.  $Q_1 \notin \mathcal{V}(E_5)$  since  $Q_1$  is above  $\pi(P_5, -e_5)$ . (b) The pair  $(E_1, Q_1)$  is considered.  $Q_1 \notin \mathcal{V}(E_1)$  since  $Q_1$  is beneath  $E_1$ . (c) The pair  $(E_5, Q_1)$  is considered.  $Q_1 \in \mathcal{V}(E_5)$ , but  $S_5 \notin \mathcal{V}(Q_1)$ .

If  $\alpha \in (0, 1)$ , then the projection lies in  $E_a$  and  $S_a$  is set to  $S$ . This case also implies that the vertex  $P_b$  is located between the lower half-planes  $\pi(P_a, -e_a)$  and  $\pi(P_{fo(a)}, e_a)$ . Therefore,

the first two relations for  $P_b$  to be an element of  $\mathcal{V}(E_a)$  are checked (compare with (17)-(19)). The last relation involves verifying whether  $P_b$  lies above the edge  $E_a$ . Let  $n_a$  be the outward normal vector to  $E_a$ . Then  $P_b$  lies above  $E_a$  if

$$\overrightarrow{P_a P_b} \cdot n_a > 0. \quad (21)$$

If this inequality is not satisfied, then  $P_b$  does not belong to  $\mathcal{V}(E_a)$  and a new pair of features must be found. This new pair is composed of  $P_b$  and the closest feature of  $R_1$  to  $P_b$ , so that the new pair is closer in distance than the previous one. Let us see how to find such a feature. Since the Voronoi regions define a partition of  $\mathbb{R}^2 \setminus R_1$ ,  $P_b$  lies either in the Voronoi region of an edge of  $R_1$  or in the Voronoi region of a vertex of  $R_1$ . On one hand,  $P_b$  lies in the Voronoi region of the edge  $E_i$  of  $R_1$  if and only if

- the projection of  $P_b$  on  $E_i$  lies in  $E_i$ , i.e.:

$$\alpha_{E_i} \in (0, 1), \quad (22)$$

- and  $P_b$  lies above the line containing  $E_i$ , i.e.:

$$\overrightarrow{P_i P_b} \cdot n_i > 0. \quad (23)$$

On the other hand,  $P_b$  lies in the Voronoi region of the vertex  $P_i$  of  $R_1$  if and only if

- the projection parameter of  $P_b$  onto  $E_{pr(i)}$ , whose endpoint is  $P_i$  is larger than 1, i.e.:

$$\alpha_{E_{pr(i)}} \geq 1, \quad (24)$$

- and the projection parameter of  $P_b$  onto  $E_i$ , whose startpoint is  $P_i$  is negative, i.e.:

$$\alpha_{E_i} \leq 0. \quad (25)$$

Therefore, to determine in which Voronoi region the point  $P_b$  belongs to, we enumerate the edges on  $R_1$  until an edge satisfies (22)-(23) or two successive edges satisfy (24)-(25). Figure 9-(b) illustrates such a case. The original pair of features is  $(E_1, Q_1)$ . The point  $Q_1$  does not belong to  $\mathcal{V}(E_1)$  since  $Q_1$  is beneath  $E_1$ . The new pair of features is  $(E_4, Q_1)$ ,  $E_4$  being the first edge of  $R_1$  that verifies (22)-(23).

It may happen that no edge satisfies (22)-(23) and no pair of successive edges verifies (24)-(25). This case means that the point  $P_b$  lies inside the polyhedron  $R_1$ . Thus, a collision between the robots is detected. The algorithm to find the feature that is the closest to  $P_b$  is summarized in Table 3.

Suppose now that  $P_b \in \mathcal{V}(E_a)$ . The last check of the case Edge-Vertex is to verify whether  $S_a \in \mathcal{V}(P_b)$ . This test corresponds to the case Vertex-Vertex since  $S_a$  and  $P_b$  are both vertices. Thus, if  $S_a \notin \mathcal{V}(P_b)$ , the feature  $P_b$  is replaced by  $E_b$  or  $E_{pr(b)}$  depending on which inequality in (16) is violated. In Figure 9-(c), an example is represented where  $Q_1 \in \mathcal{V}(E_5)$ , but the orthogonal projection  $S_5 \notin \mathcal{V}(Q_1)$ . The first inequality in (16) is here not satisfied. Then, the new candidate pair is  $(E_5, E_1)$ .

As in the case Vertex-Vertex, we relax the tests on the value of  $\alpha$  and of (21) with the positive parameter  $\delta_c$  to avoid numerical problems. Eventually, the case Edge-Vertex is summarized in Table 4.

Table 3: Algorithm “Find the Closest Feature to  $P_b$ ”

```

Compute  $\alpha_{pr} = \frac{\overrightarrow{P_m P_b} \cdot e_m}{\|e_m\|_2^2}$ 
For  $I = 1, \dots, m$ 
  Compute  $\alpha = \frac{\overrightarrow{P_I P_b} \cdot e_I}{\|e_I\|_2^2}$ 
  If  $\alpha \in [\delta_c, 1 - \delta_c]$  and  $\overrightarrow{P_I P_b} \cdot n_I > \delta_c \|n_I\|_2 \|\overrightarrow{P_I P_b}\|_2$  then
    return new pair  $(E_I, P_b)$ 
  Else if  $\alpha_{pr} > 1 - \delta_c$  and  $\alpha < \delta_c$  then
    return new pair  $(P_I, P_b)$ 
  Else
    Set  $\alpha_{pr} = \alpha$ 
  End if
End for
return collision

```

Table 4: Algorithm “Edge ( $E_a$ ) - Vertex ( $P_b$ )”

```

Compute  $\alpha = \frac{\overrightarrow{P_a P_b} \cdot e_a}{\|e_a\|_2^2}$ 
If  $\alpha > 1 - \delta_c$  then
  return new pair  $(P_{fo(a)}, P_b)$ 
Else if  $\alpha < \delta_c$  then
  return new pair  $(P_a, P_b)$ 
Else
  If  $\overrightarrow{P_a P_b} \cdot n_a < \delta_c \|n_a\|_2 \|\overrightarrow{P_a P_b}\|_2$  then
     $f_a \leftarrow$  Find the Closest Feature to  $P_b$ 
    return new pair  $(f_a, E_b)$ 
  Else
    Compute  $S_a = P_a + \alpha e_a$ 
    If  $S_a \notin \pi(P_b, e_b)$  then
      return new pair  $(E_a, E_b)$ 
    Else if  $S_a \notin \pi(P_b, e_{pr(b)})$  then
      return new pair  $(E_a, E_{pr(b)})$ 
    Else
      return  $(E_a, P_b)$  is the closest pair
    End if
  End if
End if

```

### 5.3 Case Edge-Edge

Let us consider the pair of features  $(E_a, E_b)$  where  $E_a$  is an edge of  $R_1$  and  $E_b$  is an edge of  $R_2$ . The case when the edges are parallel must be set apart from the non-parallel case.

#### 5.3.1 Parallel edges

Let us assume here that the edges  $E_a$  and  $E_b$  are parallel. Two possibilities exist. Either the edges overlap. In that case, there are several pairs of points that achieve the minimal distance between the edges. The edges may be the closest pair of features. Or, the edges do not overlap. Then, there exists a pair of vertices that are closer in distance than the pair  $(E_a, E_b)$ .

To determine if the edges overlap, the smallest edge is projected onto the largest one. Let us assume that  $\|e_b\|_2 \leq \|e_a\|_2$ . Then, the vertices  $P_b$  and  $P_{fo(b)}$  are projected onto  $E_a$ . Following (14), the projection coefficients are given by

$$\alpha_b = \frac{\overrightarrow{P_a P_b} \cdot e_a}{\|e_a\|_2^2} \quad \text{and} \quad \alpha_{fo(b)} = \frac{\overrightarrow{P_a P_{fo(b)}} \cdot e_a}{\|e_a\|_2^2}. \quad (26)$$

The edges do not overlap when  $\alpha_b, \alpha_{fo(b)}$  are both negative or both larger than 1. In that case, a new pair of features must be determined. If  $\alpha_b, \alpha_{fo(b)}$  are both negative, then  $E_b$  is closer to  $P_a$  than to  $P_{fo(a)}$ . Consequently, the first component of the new pair is  $P_a$ . For the second component, the distance between  $P_a$  and the vertices of  $E_b$  is tested. The new pair of features is

$$\begin{cases} (P_a, P_b), & \text{if } \|\overrightarrow{P_a P_b}\|_2 \leq \|\overrightarrow{P_a P_{fo(b)}}\|_2, \\ (P_a, P_{fo(b)}), & \text{otherwise.} \end{cases}$$

Similarly, if  $\alpha_b, \alpha_{fo(b)}$  are both larger than 1, the new pair of features is equal to

$$\begin{cases} (P_{fo(a)}, P_b), & \text{if } \|\overrightarrow{P_{fo(a)} P_b}\|_2 \leq \|\overrightarrow{P_{fo(a)} P_{fo(b)}}\|_2, \\ (P_{fo(a)}, P_{fo(b)}), & \text{otherwise.} \end{cases}$$

An illustration is given in Figure 10-(a). The edge  $E_2$  of  $R_1$  is parallel to  $E_3$  of  $R_2$ . The edge  $E_3$  is projected onto  $E_2$  and the resulting projection coefficients  $\alpha_1, \alpha_3$  are both larger than 1. The next pair of features is the pair of vertices  $(P_3, Q_1)$  since the vertex  $P_3$  is closer to  $P_1$  than to  $Q_3$ .

The edges overlap when at least one of the projection coefficients is in  $(0, 1)$ . All the points in the overlapping region achieve the minimum distance between the edges. However, the edges are not necessarily the closest pair of features. The edges are the closest pair, if each edge is located above the other edge. For instance, let us consider the pair of edges  $(E_1, E_1)$  in Figure 10-(b). These edges are parallel and overlap. However, they are not the closest pair of features, the edge  $E_1$  of  $R_2$  being located beneath  $E_1$  of  $R_1$ .

Let us assume that  $\alpha_b \in (0, 1)$ . The point  $S_a$  is defined as the projection of  $P_b$  onto  $E_a$ , i.e.  $S_a = P_a + \alpha_b \overrightarrow{P_a P_{fo(a)}}$ . The pair of points  $(S_a, P_b)$  achieves the minimum distance between

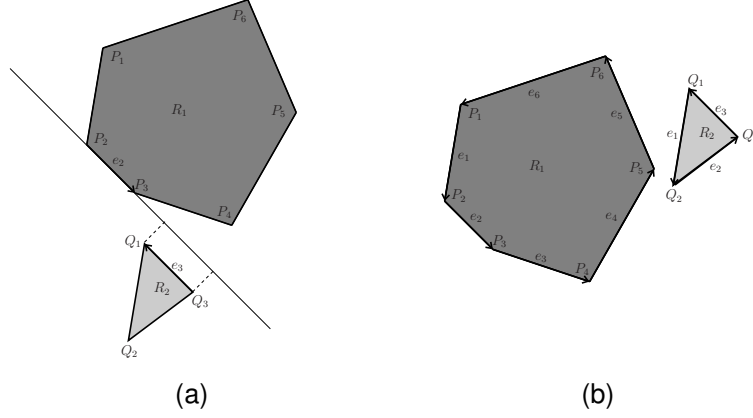


Figure 10: (a) The edges  $E_2$  of  $R_1$  and  $E_3$  of  $R_2$  are parallel and do not overlap. The pair  $(P_3, Q_1)$  is closer than  $(E_2, E_3)$ . (b) The edges  $E_1$  of  $R_1$  and  $E_1$  of  $R_2$  are parallel and overlap, but  $(E_1, E_1)$  is not the closest pair since  $E_1$  of  $R_2$  is beneath  $E_1$  of  $R_1$ .

the edges, that is,  $S_b$  is equal to  $P_b$ . According to (21), the edge  $E_a$  is above  $E_b$  if and only if the following inequality is satisfied

$$\overrightarrow{P_b P_a} \cdot n_b > 0.$$

If the inequality is not satisfied, then a new pair of features is searched. This new pair is such that the feature on  $R_1$  is the closest to  $P_b$ . The pair is obtained by applying the algorithm “Find Closest Feature to  $P_b$ ”. Similarly, we check if  $E_b$  is above  $E_a$ . If  $E_b$  is not above, then we look for the feature on  $R_2$  that is the closest to  $S_a$ . The algorithm to handle the case Edge-Edge with parallel edges is sketched in Table 5.

### 5.3.2 Non-parallel edges

Let us consider here the non-parallel case. If the edges are not parallel, then this pair of features can not be the closest pair. At least one vertex of the edges achieves the minimum distance between the edges. The goal of this section is then to find the next pair of features. This pair is composed by the features that contain the points minimizing the distance between the edges. So, let us compute the minimum distance.

Let us consider the lines that support the edges  $E_a$  and  $E_b$ :

$$\begin{aligned} \ell(e_a, P_a) &= \{x \in \mathbb{R}^2 \mid x = P_a + k_a e_a, k_a \in \mathbb{R}\}, \\ \ell(e_b, P_b) &= \{x \in \mathbb{R}^2 \mid x = P_b + k_b e_b, k_b \in \mathbb{R}\}. \end{aligned}$$

Let  $d_E$  be the distance function between any pair of points  $(S_a, S_b)$ , with  $S_a = P_a + k_a e_a \in \ell(e_a, P_a)$  and  $S_b = P_b + k_b e_b \in \ell(e_b, P_b)$ . The function  $d_E$  is defined as follows:

$$\begin{aligned} d_E : \mathbb{R} \times \mathbb{R} &\rightarrow [0, +\infty[ \\ (k_a, k_b) &\mapsto d_E(k_a, k_b) = \|P_a + k_a e_a - P_b - k_b e_b\|_2^2. \end{aligned}$$

Table 5: Algorithm “Edge ( $E_a$ ) - Edge ( $E_b$ ) parallel”, when  $\|e_b\|_2 \leq \|e_a\|_2$

```

Compute  $\alpha_b$  and  $\alpha_{fo(b)}$  as in (26)
If  $\alpha_b < \delta$  and  $\alpha_{fo(b)} < \delta$  then
  If  $\|\overrightarrow{P_a P_b}\|_2 \leq \|\overrightarrow{P_a P_{fo(b)}}\|_2$  then
    return new pair ( $P_a, P_b$ )
  Else
    return new pair ( $P_a, P_{fo(b)}$ )
  End if
Else if  $\alpha_b > 1 - \delta$  and  $\alpha_{fo(b)} > 1 - \delta$  then
  If  $\|\overrightarrow{P_{fo(a)} P_b}\|_2 \leq \|\overrightarrow{P_{fo(a)} P_{fo(b)}}\|_2$  then
    return new pair ( $P_{fo(a)}, P_b$ )
  Else
    return new pair ( $P_{fo(a)}, P_{fo(b)}$ )
  End if
Else
  If  $\alpha_b \in [\delta, 1 - \delta]$  then
    Set  $S_a = P_a + \alpha_b \overrightarrow{P_a P_{fo(a)}}$  and  $S_b = P_b$ 
  Else
    Set  $S_a = P_a + \alpha_{fo(b)} \overrightarrow{P_a P_{fo(a)}}$  and  $S_b = P_{fo(b)}$ 
  End if
  If  $\overrightarrow{P_a P_b} \cdot n_a > \delta \|n_a\|_2 \|\overrightarrow{P_a P_b}\|_2$  then
    If  $\overrightarrow{P_b P_a} \cdot n_b > \delta \|n_b\|_2 \|\overrightarrow{P_b P_a}\|_2$  then
      return ( $E_a, E_b$ ) is the closest pair
    Else
       $f_b \leftarrow$  Find the Closest Feature to  $S_a$ 
      return new pair ( $E_a, f_b$ )
    End if
  Else
     $f_a \leftarrow$  Find the Closest Feature to  $S_b$ 
    return new pair ( $f_a, E_b$ )
  End if
End if

```

The function  $d_E$  can be rewritten as

$$\begin{aligned} d_E(k_a, k_b) &= (P_a + k_a e_a - P_b - k_b e_b)^T (P_a + k_a e_a - P_b - k_b e_b), \\ &= \|e_a\|_2^2 k_a^2 - 2 e_a^T e_b k_a k_b + \|e_b\|_2^2 k_b^2 + 2 e_a^T \overrightarrow{P_b P_a} k_a - 2 e_b^T \overrightarrow{P_b P_a} k_b \\ &\quad + \|\overrightarrow{P_b P_a}\|_2^2. \end{aligned}$$

Hence,  $d_E$  is a quadratic function in  $k_a$  and  $k_b$ . Furthermore, the Hessian matrix of  $d_E$  is positive definite. Indeed, the Hessian matrix is given by

$$H(d_E)(k_a, k_b) = 2 \begin{pmatrix} \|e_a\|_2^2 & -e_a^T e_b \\ -e_a^T e_b & \|e_b\|_2^2 \end{pmatrix}.$$

On one hand, we have  $\|e_a\|_2^2 > 0$  since the edges are supposed to be not degenerate. On the other hand, the determinant of the Hessian matrix is

$$\det H(d_E)(k_a, k_b) = 4(\|e_a\|_2^2 \|e_b\|_2^2 - (e_a^T e_b)^2) = 4\|e_a\|_2^2 \|e_b\|_2^2 (1 - \cos(\beta)),$$

where  $\beta$  is the angle between  $e_a$  and  $e_b$ . Since the edges are not parallel,  $\cos(\beta) < 1$  and we deduce

$$\det H(d_E)(k_a, k_b) > 0.$$

Sylvester's criterion implies that  $H(d_E)(k_a, k_b)$  is positive definite. Consequently, the quadratic function  $d_E$  is convex.

By assumption, the lines  $\ell(e_a, P_a)$  and  $\ell(e_b, P_b)$  are not parallel. Therefore, the lines are secant and the minimum distance is equal to 0. This minimum is global since  $d_E$  is convex and quadratic. The minimum is given by solving

$$\nabla d_E(k_a, k_b) = \begin{pmatrix} 2\|e_a\|_2^2 k_a - 2e_a^T e_b k_b + 2e_a^T \overrightarrow{P_b P_a} \\ 2\|e_b\|_2^2 k_b - 2e_a^T e_b k_a - 2e_b^T \overrightarrow{P_b P_a} \end{pmatrix} = \begin{pmatrix} 0 \\ 0 \end{pmatrix}.$$

The solution of the above linear system is

$$k_a^* = \frac{(e_a^T e_b) e_b^T \overrightarrow{P_b P_a} - \|e_b\|_2^2 e_a^T \overrightarrow{P_b P_a}}{\|e_a\|_2^2 \|e_b\|_2^2 - (e_a^T e_b)^2}, \quad (27)$$

$$k_b^* = \frac{\|e_a\|_2^2 e_b^T \overrightarrow{P_b P_a} - (e_a^T e_b) e_a^T \overrightarrow{P_b P_a}}{\|e_a\|_2^2 \|e_b\|_2^2 - (e_a^T e_b)^2}. \quad (28)$$

The denominator of the above fractions is always positive since it is equal to the quarter of the determinant of the Hessian matrix, which is positive definite.

In conclusion, the lines  $\ell(e_a, P_a)$  and  $\ell(e_b, P_b)$  crosses at  $P_a + k_a^* e_a = P_b + k_b^* e_b$  and it follows

$$d_E(k_a^*, k_b^*) = 0.$$

We look for the pair of points that minimizes the distance between the edges  $E_a$  and  $E_b$ . Therefore, the minimum is no longer searched in  $\mathbb{R}^2$ , but only in  $[0, 1]^2$ . This minimum is obtained by

solving the following problem

$$(Pd_E) \quad \min d_E(k_a, k_b) \\ \text{s.t.} \quad 0 \leq k_a \leq 1, \\ 0 \leq k_b \leq 1.$$

Let  $(\bar{k}_a, \bar{k}_b)$  be the solution of  $(Pd_E)$ . If  $(\bar{k}_a, \bar{k}_b)$  lies in  $(0, 1)^2$ , then the edges intersect and a collision is detected. Indeed,  $(\bar{k}_a, \bar{k}_b) \in (0, 1)^2$  means that the minimum of  $(Pd_E)$  is achieved by points located in the edges. Since the edges are not parallel and we work in a two-dimensional space, these points necessarily coincide.

If, on the other hand,  $(\bar{k}_a, \bar{k}_b) \notin (0, 1)^2$ , then the solution of  $(Pd_E)$  is on the boundary of  $[0, 1]^2$ . To find this solution, let us consider the location of the global optimum  $(k_a^*, k_b^*)$  in  $\mathbb{R}^2$ . The value of  $d_E$  at  $(k_a^*, k_b^*)$  is null. Furthermore, the contour lines of  $d_E$  are ellipses centered at  $(k_a^*, k_b^*)$ . The value of the contour lines increases as one moves away from  $(k_a^*, k_b^*)$ .

Now, two cases must be distinguished, according to the values of  $k_a^*$  and  $k_b^*$ :

- case 1: either  $k_a^*$  or  $k_b^*$  is in  $[0, 1]$ ,
- case 2:  $k_a^*$  and  $k_b^*$  are both outside  $[0, 1]$ .

Let us start with case 1. An instance of this case is  $k_a^* > 1$  and  $k_b^* \in [0, 1]$ . For this instance, there exists a contour line that is tangent to the line  $k_a = 1$ . Let  $P_I$  be the intersection point and let  $k_b^I$  be the second coordinate of  $P_I$ , that is  $P_I = (1, k_b^I)$ . By definition of the contour lines, the value of  $d_E$  along  $k_a = 1$  is such that

$$d_E(1, k_b^I) < d_E(1, k_b), \quad \forall k_b \in \mathbb{R} \setminus \{k_b^I\}.$$

If  $k_b^I$  lies in  $[0, 1]$ , then  $(1, k_b^I)$  is the solution of  $(Pd_E)$ . If  $k_b^I$  is larger than 1, then  $P_I$  does not belong to  $\partial[0, 1]^2$ . Since the value of  $d_E$  increases from  $P_I$  to 0 along the line  $k_a = 1$ , the minimum of  $(Pd_E)$  is located at  $(1, 1)$ . Similarly, if  $k_b^I$  is smaller than 0, the minimum of  $(Pd_E)$  occurs at  $(1, 0)$ .

An illustration of the contour lines is given in Figure 11-(a). This example corresponds to the pair of edges  $(E_4, E_1)$  given in Figure 10-(b). The x-axis is the value of  $k_a$  and  $k_b$  is represented in the y-axis. The intersection point  $P_I$  is located on the boundary of  $[0, 1]^2$ .  $P_I$  achieves then the minimum of  $(Pd_E)$ .

From a mathematical point of view, the solution  $(\bar{k}_a, \bar{k}_b)$  of  $(Pd_E)$  is computed in the following manner. Because  $k_a^* > 1$ ,  $\bar{k}_a$  is set to 1. The problem now is to find a value for  $\bar{k}_b$ . The variable  $\bar{k}_b$  is found by solving

$$\min_{0 \leq k_b \leq 1} g_1(k_b) \tag{29}$$

where

$$g_1(k_b) = d_E(1, k_b) = \|e_b\|_2^2 k_b^2 - 2 e_b^T (e_a + \overrightarrow{P_b P_a}) k_b + (e_a + \overrightarrow{P_b P_a})^2.$$

The function  $g_1$  is a second-order polynomial. The minimum is obtained at the root of the first derivative of  $g_1$ :

$$g_1'(k_b) = 0 \Leftrightarrow k_b = \frac{e_b^T(e_a + \overrightarrow{P_b P_a})}{\|e_b\|_2^2}.$$

Thus, the intersection point  $P_I$  is  $(1, k_b^I)$ , where  $k_b^I$  is given by the above expression. The minimum of  $(Pd_E)$  is then obtained at

$$(\bar{k}_a, \bar{k}_b) = \begin{cases} (1, 0) & \text{if } k_b^I < 0, \\ (1, k_b^I) & \text{if } k_b^I \in [0, 1], \\ (1, 1) & \text{if } k_b^I > 1. \end{cases}$$

The pair  $(\bar{k}_a, \bar{k}_b)$  defines the pair of points  $(P_a + \bar{k}_a e_a, P_b + \bar{k}_b e_b)$ . These points indicate the next pair of features. For instance, if  $P_a + \bar{k}_a e_a$  is in the edge  $E_a$ , then the next feature is  $E_a$ . If, in the other hand,  $P_a + \bar{k}_a e_a$  is an endpoint of the edge, then the next feature is the endpoint itself. Finally, the next pair of features is defined as follows

$$\begin{cases} (P_{fo(a)}, P_b) & \text{if } (\bar{k}_a, \bar{k}_b) = (1, 0), \\ (P_{fo(a)}, E_b) & \text{if } (\bar{k}_a, \bar{k}_b) = (1, k_b^I), \\ (P_{fo(a)}, P_{fo(b)}) & \text{if } (\bar{k}_a, \bar{k}_b) = (1, 1). \end{cases}$$

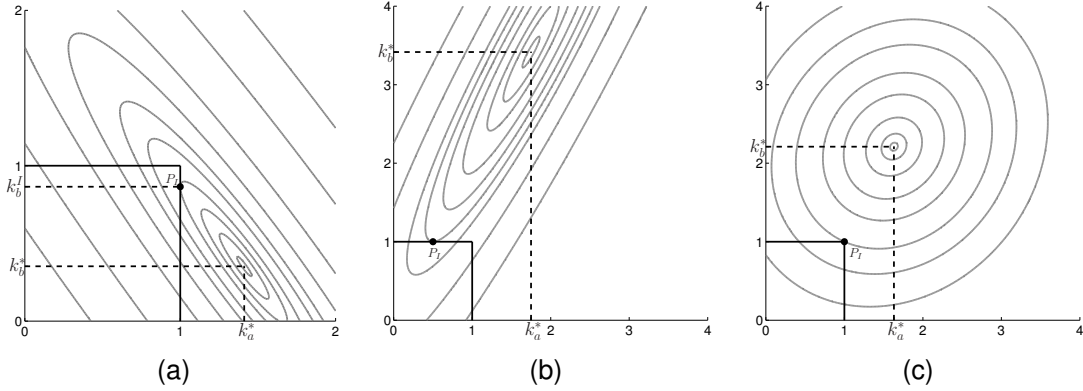


Figure 11: Contour lines of the minimum distance  $d_E$  for the pairs (a)  $(E_4, E_1)$ , (b)  $(E_5, E_3)$  and (c)  $(E_3, E_1)$  represented in Figure 10-(b). For these examples, the point  $P_I$  achieves the minimum of  $(Pd_E)$ .

The other instances of case 1 are  $(k_a^*, k_b^*) \in ]-\infty, 0[ \times [0, 1]$ ,  $(k_a^*, k_b^*) \in [0, 1] \times ]1, +\infty[$  and  $(k_a^*, k_b^*) \in [0, 1] \times ]-\infty, 0[$ . They are handled similarly. For example, the instance  $(k_a^*, k_b^*) \in ]-\infty, 0[ \times [0, 1]$  is solved by setting  $\bar{k}_a$  to 0 and  $\bar{k}_b$  to the solution of

$$\min_{0 \leq k_b \leq 1} g_0(k_b) = d_E(0, k_b).$$

Now, let us consider case 2. This case contains the instances  $k_a^*, k_b^* > 1$ ,  $k_a^*, k_b^* < 0$ ,  $k_a^* > 1, k_b^* < 0$  and  $k_a^* < 0, k_b^* > 1$ . Let us study the first instance, i.e.  $k_a^*, k_b^* > 1$ . The Figures 11-(b) and 11-(c) illustrate such a case. Figure 11-(b) corresponds to the pair  $(E_5, E_3)$ . The contour

line hits first the segment line  $[0, 1] \times \{1\}$ . The minimum is then reached at  $(\bar{k}_a, 1)$  with  $\bar{k}_a \in (0, 1)$ . The next candidate pair of features is  $(E_5, P_1)$ . Figure 11-(c) illustrates the contour lines of the distance function  $d_E$  for the pair  $(E_3, E_1)$  in Figure 10-(b). The contour line hits the corner  $(1, 1)$  of the square  $[0, 1]^2$ . Hence,  $(1, 1)$  achieves the minimum of  $d_E$  on  $[0, 1]^2$  and the next candidate pair is  $(P_4, P_2)$ .

Mathematically, the minimum of  $(Pd_E)$  is computed in a similar way to case 1. The additional difficulty here is how to determine which from  $\bar{k}_a$  and  $\bar{k}_b$  must be initially set to 1. One possibility is to evaluate the sign of the partial derivatives at the corner  $(1, 1)$ . However we prefer to simply apply the above computations to  $\bar{k}_a = 1$ , then to  $\bar{k}_b = 1$  and compare the resulting pairs of points. More precisely, let us first set the parameter  $\bar{k}_{a,1}$  to 1. We associate here the index 1 to indicate that we compute the first pair. Then, by solving (29), the pair  $(\bar{k}_{a,1}, \bar{k}_{b,1})$  is obtained. To this pair of parameters corresponds the pair of points  $(P_a + \bar{k}_{a,1}e_a, P_b + \bar{k}_{b,1}e_b)$ .

In a second step, the parameter  $\bar{k}_{b,2}$  is set to 1 and  $\bar{k}_{a,2}$  is the solution of the following minimization problem

$$\bar{k}_{a,2} = \arg \min_{0 \leq k_a \leq 1} d_E(k_a, 1).$$

The second pair of points is  $(P_a + \bar{k}_{a,2}e_a, P_b + \bar{k}_{b,2}e_b)$ . The minimum of  $(Pd_E)$  occurs at the closest pair of points, i.e. at

$$(\bar{k}_a, \bar{k}_b) = \begin{cases} (\bar{k}_{a,1}, \bar{k}_{b,1}) & \text{if } d_E(\bar{k}_{a,1}, \bar{k}_{b,1}) \leq d_E(\bar{k}_{a,2}, \bar{k}_{b,2}), \\ (\bar{k}_{a,2}, \bar{k}_{b,2}) & \text{otherwise.} \end{cases} \quad (30)$$

The next pair of features is deduced from  $(\bar{k}_a, \bar{k}_b)$ , as previously:

$$\begin{cases} (P_a + \bar{k}_a e_a, P_b + \bar{k}_b e_b) & \text{if } \bar{k}_a, \bar{k}_b \in \{0, 1\}, \\ (E_a, P_b + \bar{k}_b e_b) & \text{if } \bar{k}_a \in (0, 1), \bar{k}_b \in \{0, 1\}, \\ (P_a + \bar{k}_a e_a, E_b) & \text{if } \bar{k}_a \in \{0, 1\}, \bar{k}_b \in (0, 1). \end{cases}$$

We can observe that the next pair of features always contains at least one vertex. The case Edge-Edge when the edges are not parallel is summarized in the algorithm of Table 6.

## 5.4 Convergence

The convergence of Lin and Canny's algorithm is guaranteed since the new pair of features is always closer in distance than the previous pair. Furthermore, the test algorithms "Vertex  $(P_a)$  - Vertex  $(P_b)$ ", "Edge  $(E_a)$  - Edge  $(E_b)$ ", "Edge  $(E_a)$  - Edge  $(E_b)$  parallel" and "Edge  $(E_a)$  - Edge  $(E_b)$  not parallel" are constant in time. Only the convergence of the algorithm "Find the closest feature to  $P_b$ " is of order  $m$ , the number of vertices in the robot. In the worst case, the  $4m^2$  possible pairs of features are visited. Consequently, Lin and Canny's algorithm is  $O(m^3)$ . However, the order of the method can be drastically reduced, when the initial pair is well chosen. In our particular application, the robots move slightly between two consecutive time steps  $t_k$  and  $t_{k+1}$ . In this case, a good initial pair at  $t_{k+1}$  is the closest pair of features found at  $t_k$ . The closest pair at  $t_{k+1}$  is then either the initial pair itself or a neighboring pair, that is obtained by applying the constant in time test algorithms.

Table 6: Algorithm “Edge ( $E_a$ ) - Edge ( $E_b$ ) not parallel”

```

Compute  $k_a^*$  and  $k_b^*$  according to (27)-(28)
If  $(k_a^*, k_b^*) \in [0, 1]^2$  then
    return collision
Else if  $k_a^* \in [0, 1]$  then
    If  $k_b^* > 1$  then
        Set  $\bar{k}_b = 1$  and  $\bar{k}_a = \arg \min_{0 \leq k_a \leq 1} d_E(k_a, 1)$ 
    Else
        Set  $\bar{k}_b = 0$  and  $\bar{k}_a = \arg \min_{0 \leq k_a \leq 1} d_E(k_a, 0)$ 
    End if
Else if  $k_b^* \in [0, 1]$  then
    If  $k_a^* > 1$  then
        Set  $\bar{k}_a = 1$  and  $\bar{k}_b = \arg \min_{0 \leq k_b \leq 1} d_E(1, k_b)$ 
    Else
        Set  $\bar{k}_a = 0$  and  $\bar{k}_b = \arg \min_{0 \leq k_b \leq 1} d_E(0, k_b)$ 
    End if
Else
    Compute  $(\bar{k}_a, \bar{k}_b)$  as in (30)
End if
If  $\bar{k}_a, \bar{k}_b \in \{0, 1\}$  then
    return new pair  $(P_a + \bar{k}_a e_a, P_b + \bar{k}_b e_b)$ 
Else if  $\bar{k}_a \in (0, 1)$  then
    return new pair  $(E_a, P_b + \bar{k}_b e_b)$ 
Else
    return new pair  $(P_a + \bar{k}_a e_a, E_b)$ 
End if

```

## 6 Numerical results

The collision detection algorithm is applied to the two-dimensional work-cell presented in Figure 12. The work-cell is composed of four obstacles (black quadrilaterals) and two robots  $R_1$  and  $R_2$ . The robot  $R_1$  is depicted at several time steps by a light grey square. The robot starts from  $V_I^1$ , follows the light grey trajectory and ends at  $V_F^1$  (black triangle). The markers on the trajectory indicate the position of the center of gravity of  $R_1$  at the time steps  $\tau_k$ ,  $k = 1, \dots, n$ . Similarly, the robot  $R_2$  is the dark grey square and its associated trajectory is the dark grey curve. The robot  $R_2$  moves from  $V_I^2$  to  $V_F^2$ .

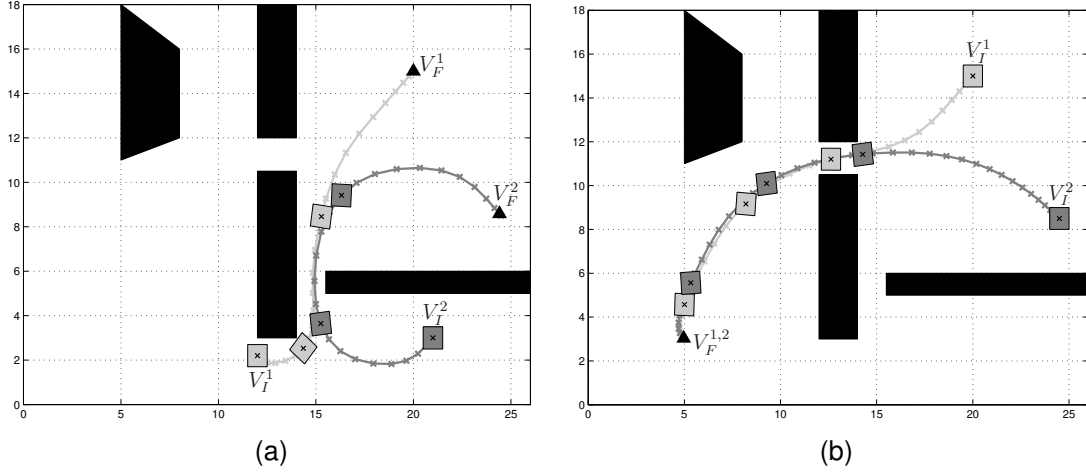


Figure 12: A two-dimensional work-cell. The black quadrilaterals are the obstacles. The grey squares are the robots, represented at several time steps. The robot  $R_1$  is light grey and the robot  $R_2$  is dark grey. The associated trajectories follow the same color code. The black diamonds are the end point of the trajectories. (a) the trajectories are collision-free. (b) the robots intersect just before reaching the end position  $V_F^{1,2}$ .

For the numerical example given in Figure 12-(a), the collision detection algorithm correctly returns that the robots do not intersect. The example is composed of 52 time intervals of the form  $[t_l, t_u]$ . Only one interval is split into two subintervals while checking Schwarzzer et al.'s inequality. The upper bound  $\eta$  of the distance between the robots is mostly computed in the broad phase, even if the robots are close to each other while travelling along the trajectories. The narrow phase is called only 7 times. For these 7 instances, only 14 test algorithms of Lin and Canny's method are applied.

In the example in Figure 12-(b), both robots have the same end point, denoted by  $V_F^{1,2}$ . Hence, the robots collide. Moreover, the trajectories are such that the robots follow each other very closely. With these trajectories, the detection algorithm must consider 71 time intervals  $[t_l, t_u]$ . The collision is detected while checking Schwarzzer et al.'s inequality for the 56<sup>th</sup> time interval. The robots at the end time of this interval are depicted in Figure 12-(b). We can observe that the robots intersect just before reaching  $V_F^{1,2}$ . Before the collision is detected, about 30 time intervals and subintervals are bisected. Lin and Canny's algorithm is called 9 times and the test algorithms are applied 12 times.

These two examples illustrate the good running of our collision detection algorithm. The algorithm returns the good solution and always almost instantaneously. Indeed, the CPU time is equal to  $4 \cdot 10^{-3}$  s for the first example, and to  $5 \cdot 10^{-3}$  s for the second example. Lin and Canny's algorithm is also well adapted to our two-dimensional examples since the number of calls to the test algorithms is small. Finally, the few calls to the narrow phase shows the good estimation of the lower bound  $\lambda_1$  and  $\lambda_2$  in Schwarzer et al.'s inequality. We conclude, that the collision detection algorithm is perfectly suited for the second step of the iterative method to solve (WCP).

## 7 Conclusions

An algorithm to detect a collision between robots moving along specified trajectories has been presented. This algorithm is used to solve the work-cell problem (WCP) described in [13]. Therefore, the robots are two-dimensional convex polyhedra.

The collision detection algorithm follows the dynamic method developed by Schwarzer et al. in [24]. The method involves comparing lower bounds of the distance travelled by the robots during a time interval, with an upper bound of the distance between the robots. We have established a formula of the lower bounds that perfectly suits the robots and the trajectories issued from (WCP). To compute the upper bound of the distance, when the robots are close to each other, we have adapted Lin and Canny's algorithm to our two-dimensional case. The resulting algorithm was applied to the second step of the iterative method to solve (WCP). Numerical examples have shown the efficiency of the algorithm: a correct output is given almost instantaneously.

These good results encourage us to use the same strategy for a three-dimensional work-cell that contains industrial robots. However, due to the complexity of the geometry of such robot, a bounding volume hierarchy method must be included to compute the right hand side of Schwarzer et al.'s inequality efficiently.

## References

- [1] J. W. Boyse. Interference detection among solids and surfaces. *Commun. ACM*, 22(1):3–9, 1979.
- [2] S. Cameron. A study of the clash detection problem in robotics. In *Int. Conf. Robotics & Automation*, pages 488–493, 1985.
- [3] S. Cameron. Enhancing GJK: Computing minimum and penetration distances between convex polyhedra. In *Proceedings of International Conference on Robotics and Automation*, pages 3112–3117, 1997.
- [4] J. Canny. Collision detection for moving polyhedra. Technical report, Massachusetts Institute of Technology, October 1984.

- [5] J. D. Cohen, M. C. Lin, D. Manocha, and M. K. Ponamgi. I-collide: An interactive and exact collision detection system for large-scaled environments. In *Symposium on Interactive 3D Graphics*, pages 189–196. ACM Siggraph, April 1995.
- [6] D. P. Dobkin and D. G. Kirkpatrick. Fast detection of polyhedral intersection. *Journal of Algorithm*, 6, issue 3:381–392, 1985.
- [7] M. Gerds, R. Henrion, D. Hömberg, and C. Landry. Path planning and collision avoidance for robots. *Numerical Algebra, Control and Optimization*, 2(3):437 – 463, 2012.
- [8] E.G. Gilbert and S.M. Hong. A new algorithm for detecting the collision of moving objects. In *IEEE Proc. Int. Conf. Robotics Automat.*, volume 1, pages 8–14, 1989.
- [9] E.G. Gilbert, D.W. Johnson, and S.S. Keerthi. A fast procedure for computing the distance between complex objects in three-dimensional space. *IEEE Journal of Robotics and Automation*, 4(2):193–203, April 1988.
- [10] S. Gottschalk, M. C. Lin, and D. Manocha. Obb-tree: A hierarchical structure for rapid interference detection. In ACM SIGGRAPH, editor, *Computer Graphics Proceedings, Annual Conference Series*, 1996.
- [11] P. M. Hubbard. Approximating polyhedra with spheres for time-critical collision detection. *ACM Transactions on Graphics*, 15:179–210, 1996.
- [12] P. Jiménez, F. Thomas, and C. Torras. 3d collision detection: A survey. *Computers and Graphics*, 25:269–285, April 2000. Preprint submitted to Elsevier Preprint.
- [13] C. Landry, R. Henrion, D. Hömberg, M. Skutella, and W. Welz. Task assignment, sequencing and path-planning in robotic welding cells. In *Methods and Models in Automation and Robotics (MMAR), 2013 18th International Conference on*, pages 252–257, 2013.
- [14] E. Larsen, S. Gottschalk, M. C. Lin, and D. Manocha. Fast distance queries with rectangular swept sphere volumes. In *Proc. of IEEE Int. Conference on Robotics and Automation*, pages 3719–3726, 2000.
- [15] S. M. LaValle. *Planning Algorithms*. Cambridge University Press, Cambridge, U.K., 2006.
- [16] M. C. Lin. *Efficient Collision Detection for Animation and Robotics*. PhD thesis, Department of Electrical Engineering and Computer Science, University of California, Berkeley, 1993.
- [17] M. C. Lin and J. F. Canny. A fast algorithm for incremental distance calculation. *Robotics and Automation, 1991. Proceedings., 1991 IEEE International Conference on*, page 1008, 1991.
- [18] M. C. Lin and S. Gottschalk. Collision detection between geometric models: A survey. In *In Proc. of IMA Conference on Mathematics of Surfaces*, pages 37–56, 1998.
- [19] K. Maruyama. A procedure to determine intersections between polyhedral objects. *International Journal of Computer & Information Sciences*, 1:255–266, 1972.

- [20] B. Mirtich. V-clip: Fast and robust polyhedral collision detection. Technical report, Mitsubishi Electronics Research Laboratory, 1997.
- [21] B. Mirtich. Efficient algorithms for two-phase collision detection. In K. Gupta and A.P. del Pobil, editors, *Practical Motion Planning in Robotics: Current Approaches and Future Directions*, pages 203–223. Wiley, New York, 1998.
- [22] S. Quinlan. Efficient distance computation between nonconvex objects. In *Proceedings IEEE International Conference on Robotics & Automation*, pages 3324–3329, 1994.
- [23] S. Redon, A. Kheddar, and S. Coquillart. An algebraic solution to the problem of collision detection for rigid polyhedral objects. In *Proceedings of the 2000 IEEE International Conference on Robotics and Automation, ICRA 2000, April 24-28, 2000, San Francisco, CA, USA*, pages 3733–3738. IEEE, 2000.
- [24] F. Schwarzer, M. Saha, and J. Latombe. Adaptive dynamic collision checking for single and multiple articulated robots in complex environments. *IEEE Tr. on Robotics*, 21:338–353, 2005.
- [25] P. Toth and D. Vigo. The vehicle routing problem. pages 1–26. Society for Industrial and Applied Mathematics, Philadelphia, PA, USA, 2001.